A fast preliminary estimation model for transoceanic tsunami propagation

Modesto Ortiz[1], E. Gómez-Reyes[2], and H.S. Vélez-Muñoz[2]

[1]***Departamento de Oceanografía, CICESE, Ensenada, Baja California, México***
[2]***Ingeniería de Procesos e Hidráulica, UAM, México, D.F., México***

Abstract. A simplified one-dimensional method is proposed to estimate the height of the leading wave of transoceanic tsunamis by means of a directivity function applied to the one-dimensional finite difference model based on the shallow water equations. The numerical modeling of the 4 October 1994 Shikotan tsunami, and the analysis of its deep-ocean signature observed at a distance of ∼6300 km from the source, as well as the analysis of the linear shallow water equations (non-dispersive theory) and of the Boussinesq equations (dispersive theory), shows that the frequency dispersion mechanism, as prescribed by Boussinesq equations, is a necessary and sufficient condition to simulate the transoceanic propagation of tsunamis. The analytical results from non-dispersive equations, as compared with those obtained using dispersive theory, overestimate significantly the height of the leading wave of large and medium size tsunamis. The results confirm that the linear shallow water equations solved by an explicit central finite difference method are appropriate to simulate the tsunami propagation from the source area to the far field. This is due to the fact that the inherent frequency dispersion in the numerical method mimics the frequency dispersion prescribed by Boussinesq equations (Imamura *et al.,* 1990; Liu *et al.*, 1995).

1. Introduction

We reexamine the equations that govern transoceanic tsunami propagation in order to evaluate flooding risk for coastal regions after a tsunami warning. Since 1960, only the 1960 Chile and the 1964 Alaska tsunamis have caused damage across the Pacific Ocean basin. However, between 1991 and 1997, 13 warnings were issued by the Pacific Tsunami Warning Center (Blackford, 1999). The warning from the 4 October 1994 Shikotan tsunami caused panic along the Pacific coasts of North, Central, and South America, mainly because of the lack of a reliable criterion to evaluate the risk of potential flooding. A reliable criterion for evaluating tsunami warnings might consist in a database of numerical simulations of transoceanic tsunami propagations from generation regions. However, before beginning to create such a database, it is worthwhile to reexamine the governing equations of tsunami propagation as well as the methods of solution.

The appropriate governing equations have been a subject of debate over the last three decades (Tuck, 1979). This is due to differences in the predicted height of the leading wave when using linear shallow water equations, or linear Boussinesq equations. For long propagation distances (far from the source area), the frequency dispersion from Boussinesq equations reduces the height of the leading wave as compared with the height obtained by using the shallow water equations. The difference may be of a few centimeters in

[1]CICESE-Oceanologia, Km 107 Carretera Tijuana-Ensenada, Ensenada, Baja California 22860, México (ortizf@cicese.mx)
[2]Ingeniería de Procesos e Hidráulica, UAM, México, D.F., México

the deep ocean, but it could be significant in the estimation of tsunami run-up. For near-field tsunamis, in a sea deeper than 50 m, the linear long-wave theory is said to be adequate for practical purposes; and in a sea shallower than 50 m, the shallow-water theory including bottom friction is normally used (Shuto *et al.*, 1991). In some cases the single estimation of the leading-wave height could be misleading in terms of the risk of maximum potential flooding since the second, third, or fourth waves can be higher than the leading one, as in the 1964 Hilo tsunami (Fig. 12), where the second wave was higher than the leading wave.

Houston (1978) and Houston *et al.* (1984) concluded that linear long-wave equations govern the generation and propagation over the deep ocean and the continental shelf of the leading tsunami wave. They suggested that for very large tsunamis, such as the 1964 Alaska tsunami, frequency dispersion is negligible during propagation except when tsunamis exhibit a bore-like shape in their final run-up phase. Hammack and Segur (1978) agreed that for large tsunamis, nonlinearity or frequency dispersion have no significant effect on the leading wave. Kowalik (1993) proposed a Fourth-Order Leapfrog scheme to smoothen the effect of dispersion introduced by numerical solutions of the shallow water equations. On the other hand, Heinrich *et al.* (1998) found that the effect of dispersion can be significant. They solved the Boussinesq equations using the finite difference method. Imamura *et al.* (1990) and Liu *et al.* (1995) also considered this effect as important. By choosing an appropriate grid size and a time step in the finite difference method, they were able to mimic the frequency dispersion prescribed by Boussinesq. Yoon and Liu (1993), proposed a similar method using finite elements.

The mechanism of frequency dispersion is not clearly established from tsunami observations at coastal tide gauges, due to the strong influence of local bathymetry and topography on the wave field. Thus the establishment and validation of the appropriate governing equations for transoceanic tsunami propagation is still debated. In this paper, the deep-ocean signature of the 4 October 1994 Shikotan tsunami is analyzed to assess the effect of frequency dispersion. For the governing equation selected here, we propose a one-dimensional model for tsunami propagation that can be used to evaluate the flood risk within minutes after a tsunami warning, provided that the local response, bathymetry, and topography are well known for each location in advance.

2. Deep-Ocean Signature of the 4 October 1994 Shikotan Tsunami

The Pacific Marine Environmental Laboratory (PMEL/NOAA) has developed a long-term monitoring network of bottom pressure recorder (BPR) stations in the Pacific Ocean with sea-level sensitivity of 1 mm (González *et al.*, 1987; Eble and González, 1991; Eble *et al.*, 1989). We analyze the data from one BPR, which contains a record of the deep-ocean signature of the 4 October 1994 Shikotan tsunami at a sampling rate of 15 s. The BPR is

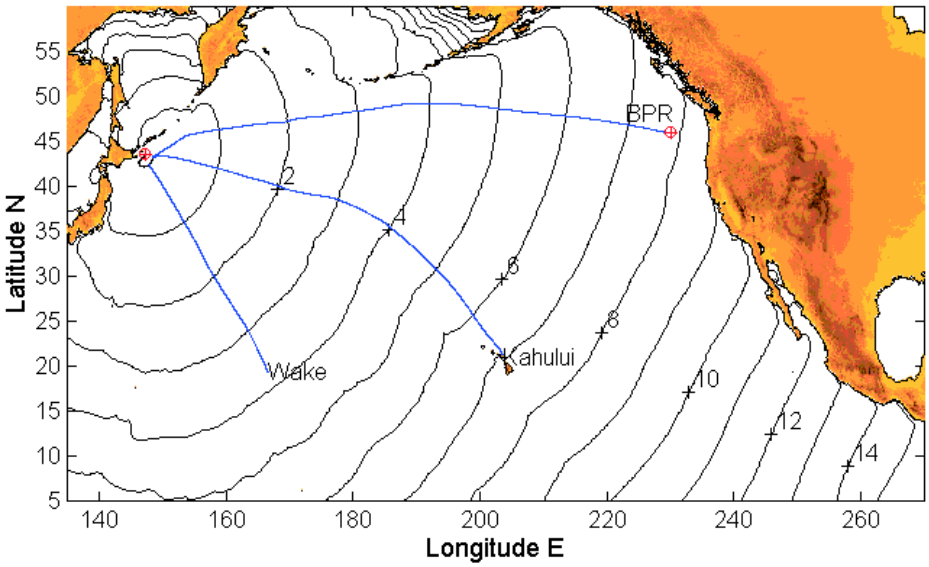

Figure 1: Travel-time chart (in hours) estimated by the two-dimensional numerical simulation of the 4 October 1994 Shikotan tsunami. The lines connecting the tsunami source with Kahului Bay, Wake Island, and the BPR location are the paths S of minimum travel time to each location.

located about 450 km offshore in the northeast Pacific (45.95°N, 129.99°W), at a depth of 1550 m and approximately at a distance of 6300 km from the tsunami source (Fig. 1).

A comprehensive analysis requires the estimation of the tsunami path (S) from the source to the BPR location, as well as the synthetic tsunami data for comparison. A preliminary numerical simulation of the Shikotan tsunami was performed using the shallow water equations (Pedlosky, 1979):

$$\begin{aligned} \frac{\partial \eta}{\partial t} + \nabla \cdot \mathrm{M} &= 0 \\ \frac{\partial \mathrm{M}}{\partial t} + gh\nabla\eta + 2\Omega \times \mathrm{M} &= 0 \end{aligned} \tag{1}$$

where t is time, η is the vertical displacement of the water surface above the normal water level, h is the ocean depth, M is the horizontal depth-averaged volume flux vector, g is the gravitational acceleration and Ω is the angular velocity of the Earth.

Equations (1) were solved in spherical coordinates using the finite difference method with a staggered leap-frog scheme (Goto *et al.*, 1997). The grid size was set to 4 min and the time step to 5 s. The bathymetry was taken from the ETOPO-2 data bank (Smith and Sandwell, 1997). The rupture parameters of the 4 October 1994 earthquake were taken from Kikuchi and Kanamori (1995), considering a steep fault (strike, dip, rake) = (49°, 75°, 125°), and a uniform dislocation of 5.6 m over the fault area of 120×60 km. The vertical movement of the sea floor was computed using the dislocation

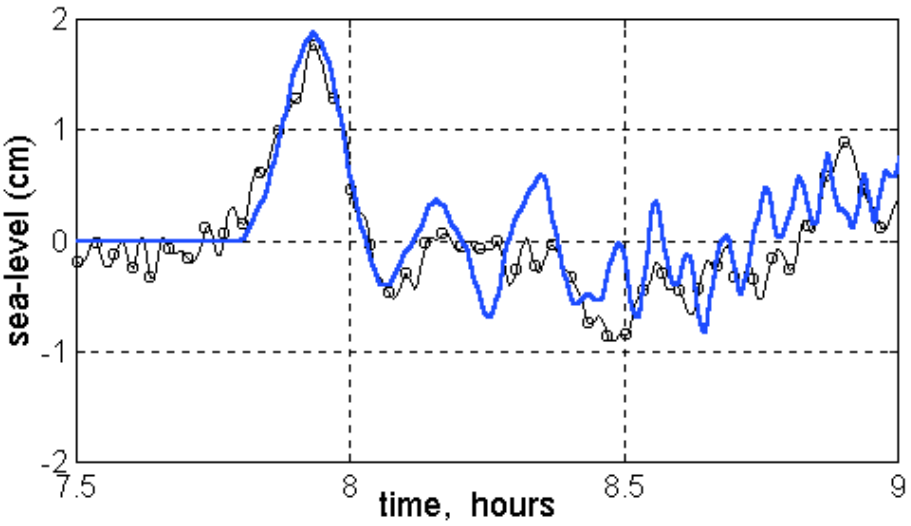

Figure 2: The 4 October 1994 Shikotan tsunami at the BPR location: Observed tsunami (line with circles) and synthetic tsunami (solid line) obtained by the two-dimensional numerical simulation. The origin of the time axis is defined as the origin time of the earthquake (13:22:58.1; UT).

model of Mansinha and Smylie (1971). As an initial condition, the sea-level change due to the rupture was taken to be the same as the instantaneous sea-floor uplift computed by the dislocation model.

The path S was obtained from the travel-time chart (Fig. 1), based on the identification of the tsunami wave front at every time step in the numerical model. Once the travel time matrix is obtained, the path can be computed as orthogonal to the wave fronts. The bathymetric profile along the path was obtained by linear interpolation from the ETOPO-2 data bank. Synthetic time series of vertical displacements of the water surface at the location of the BPR were obtained from the numerical simulation of the tsunami. Figure 2 shows the excellent agreement between the observed and synthetic tsunamis. In the synthetic tsunami, the two oscillations that follow the main peak are produced clearly by numerical dispersion. The later high-frequency waves are produced by interaction of the wave front with the bathymetry. The two subsequent oscillations are barely seen in the BPR data due to background noise.

A BPR spectrogram, where energy contours are mapped in time-frequency space, was used to estimate the evolution of tsunami energy as a function of time and frequency (Fig. 3a). The spectrogram, z, was computed using the complex demodulation concept (Ortiz, 2000):

$$z\left(f=\frac{f_N}{a},t\right)=\frac{f_N}{a\sqrt{2\pi}}\int_{-\infty}^{\infty}\eta(\tau)e^{-(t-\tau)^2(f_N/2a)^2}e^{-i2\pi f_N(t-\tau)/a}d\tau \qquad (2)$$

In (2), $f=\omega/2\pi$ is the cyclic frequency, ω is the angular frequency,

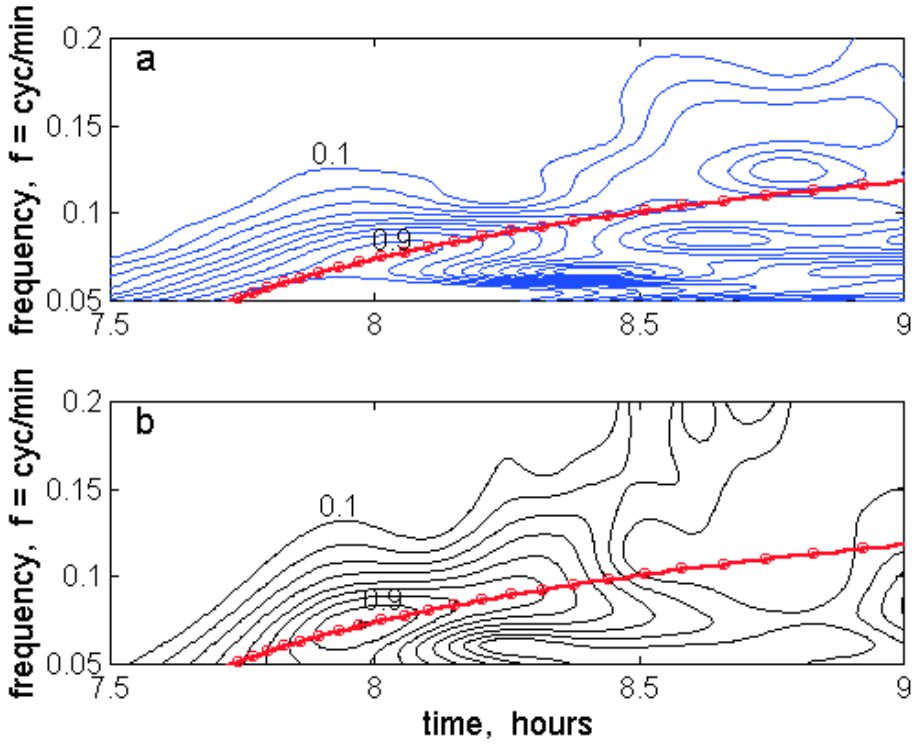

Figure 3: (a) Spectrogram of the BPR data and (b) spectrogram of the synthetic tsunami. Energy contours in both spectrograms are normalized by the maximum value. The trace of the arrival time function $t_a(f)$ is indicated in both figures by the solid line with circles. The origin of the time axis is defined as the origin time of the earthquake.

and f_N the Nyquist frequency. The parameter, a, controls the width of the bandpass filters employed in the demodulation.

Frequency dispersion in the BPR spectrogram is indicated by the curvature of the energy ridge. A similar dispersive pattern can be observed in the spectrogram of the synthetic tsunami (Fig. 3b). The energy ridge in the BPR spectrogram reproduces well the arrival as a function of frequency, $t_a(f)$, as prescribed by the linear Boussinesq equations (Liu *et al.*, 1995):

$$\begin{aligned} \frac{\partial \eta}{\partial t} + \nabla \cdot \mathrm{M} &= 0 \\ \frac{\partial \mathrm{M}}{\partial t} + gh\nabla\eta + 2\Omega \times \mathrm{M} &= \nabla \left[\frac{h^3}{3} \frac{\partial}{\partial t} \nabla \cdot \left(\frac{\mathrm{M}}{h} \right) \right]. \end{aligned} \tag{3}$$

The arrival time for each frequency was computed from the equation

$$t_a(f) = \int_s \frac{dS}{C_g(f,S)} \,, \tag{4}$$

where $C_g(f,S)$ is the group velocity derived from the one-dimensional form of (3) along the path from the tsunami source (43.48°N, 147.40°E) to the location of the BPR:

$$C_g(f,S) = \frac{\sqrt{gh(S)}\left(3-2k^2h^2(S)\right)}{3\sqrt{1-k^2h(S)^2/3}}$$
$$f = \frac{k}{2\pi}\sqrt{(1-k^2h^2(S)/3)\,gh(S)} \quad , \tag{5}$$

where k is the wave number.

The trace of the arrival time $t_a(f)$ is well reproduced by the spectrogram of the synthetic tsunami (Fig. 3b). The Imamura number is ∼0.7 along 90% of the path; thus the numerical results mimic the frequency dispersion prescribed by the Boussinesq equations (Imamura *et al.*, 1990; Shuto *et al.*, 1991; Satake *et al.*, 1995).

In conclusion, the deep-ocean signature of the 4 October 1994 Shikotan tsunami is consistent with a frequency dispersion as computed from the Boussinesq equations. For modeling the transoceanic tsunami propagation, a higher order dispersion relationship is not required. Let us now find out whether Boussinesq dispersion is a necessary condition for large tsunamis, or whether the non-dispersive condition *wave celerity* $\approx \sqrt{gh}$ is sufficient.

3. Frequency Dispersion, a Necessary Condition for Large Tsunamis

The simulated height of the leading wave of tsunamis, from dispersive or non-dispersive theories, depends largely on the ocean depth and on the tsunami initial condition, *i.e.*, on the spectral distribution of its energy. Consider the two-dimensional propagation in a plane sheet of water of uniform depth ($h = 3000$ m) of two tsunamis of different size. A representative medium-size tsunami was selected as the largest among those which occurred in Mexico, 1985 (Anderson *et al.*, 1986), Nicaragua, 1992 (Satake *et al.*, 1993), Flores Island, 1992 (Yeh *et al.*, 1993), Shikotan, 1994 (Kikuchi and Kanamori, 1995), and Jalisco, 1995 (Ortiz *et al.*, 1998). This tsunami is assumed as being generated by a reverse fault of width $W = 70$ km, length $L = 200$ km, dip angle of 30°, slip magnitude of 4 m, and a shallow edge at a depth of 15 km. For the large tsunami, the fault parameters of the 22 May 1960 Chilean tsunami were assumed (Kanamori and Ciper, 1974; $L = 800$ km, $W = 200$ km, dip angle of 10°, slip magnitude of 24 m, shallow depth of 25 km). The two-dimensional initial conditions of large and medium size tsunamis (Figs. 4a, b) were computed from the dislocation model of Mansinha and Smylie (1971).

The transoceanic propagation was computed from both dispersive and non-dispersive theories, *i.e.*, the linear shallow water equations (1) and the linear Boussinesq equations (3), neglecting the Earth rotation. The solution of (1) and (3) in a closed plane sheet of water of uniform depth, can be

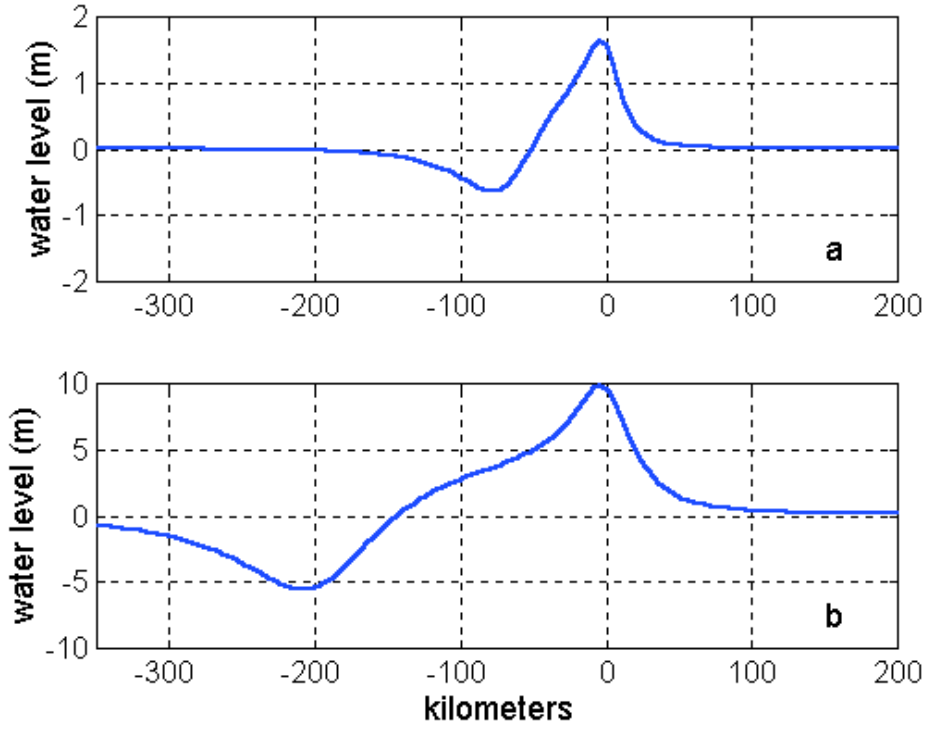

Figure 4: Two-dimensional tsunami initial condition projected along the principal axis, i.e., the axis perpendicular to the strike of the fault plane. (a) Medium size tsunami and (b) large tsunami. The tsunami initial condition was taken to be the same as the instantaneous sea-floor uplift computed by the dislocation model of Mansinha and Smylie (1971).

expressed as a single equation in rectangular coordinates ($0 \leq x \leq a$; $0 \leq y \leq b$) (Lamb, 1932):

$$\begin{aligned} \eta(x,y,t) &= \sum_m \sum_n A_{m,n} \cos(m\pi x/a) \cos(n\pi y/b) \cos(Ckt) \\ k^2 &= \pi^2(m^2/a^2 + n^2/b^2) \quad , \end{aligned} \tag{6}$$

where k is the wavenumber, C is the wave celerity, $A_{m,n}$ are the Fourier coefficients, and a and b are the length and width of the rectangular coordinate domain. The solution of (1) was obtained by setting $C = C_0 = \sqrt{gh}$, whereas the solution of (3) was obtained for the dispersion relationship

$$C = \omega/k = C_0\sqrt{1 - k^2h^2/3} \; , \tag{7}$$

After propagating 6000 km from the source, along an axis perpendicular to the strike of the fault plane (to be referred as principal axis), the height of the leading wave of the medium or large tsunami evaluated by means of the non-dispersive theory exceeded by ∼200% or ∼60% the height of the leading wave computed from dispersive theory. Differences are less than

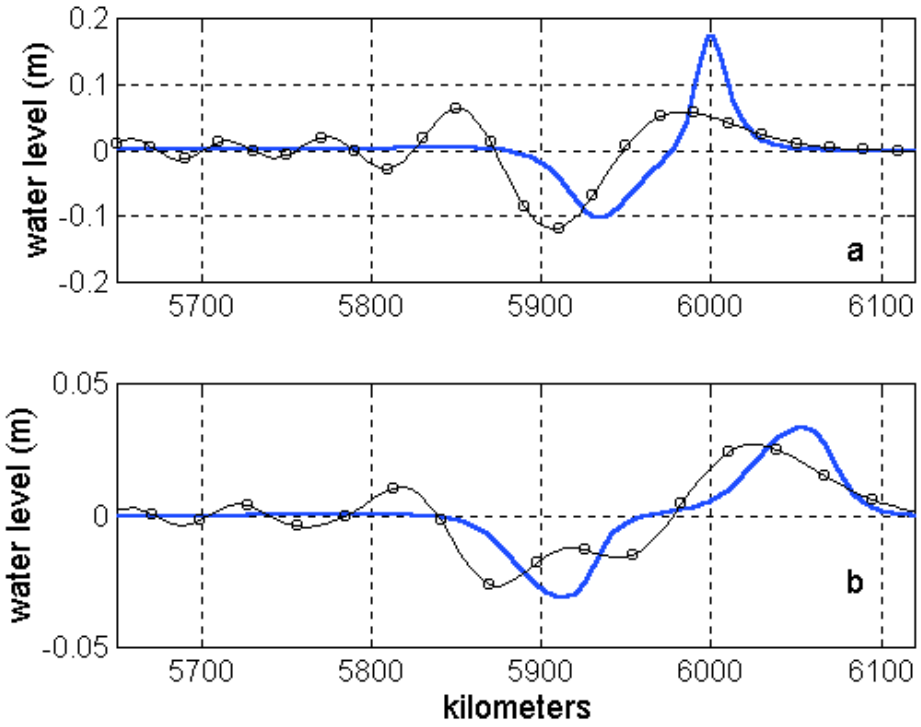

Figure 5: Medium size tsunami after being propagated a distance of 6000 km from its origin by employing dispersive theory (line with circles) and nondispersive theory (solid line). (a) Along the principal axis and (b) along the diagonal axis.

20% along the diagonal and parallel axis for both tsunamis, due to the two-dimensional geometrical spreading acting like a damping factor proportional to the propagation distance and to the wavenumber. Without dispersion, the short-wave components at the wave front, between the diagonal and parallel axis, are attenuated by the damping factor. When dispersion is acting, the short waves are left behind the wave front and are attenuated by the damping factor. This mechanism minimizes the differences in the wave height resulting from dispersive and non-dispersive theories for diagonal and parallel propagation. Along the principal axis, the tsunami directivity minimizes wave spreading, and the short wave components produce large differences in the wave front. Figures 5 (a, b) and 6 (a, b) compare the waveform of medium and large-size tsunamis, as computed using dispersive and non-dispersive theories. In order to estimate the significance of the differences in the wave height in terms of flooding, the run-up produced for both kinds of tsunamis was computed using the one-dimensional nonlinear shallow water equations

$$\begin{aligned} \frac{\partial \eta}{\partial t} + \frac{\partial \mathrm{M}}{\partial t} &= 0 \\ \frac{\partial \mathrm{M}}{\partial t} + \frac{\partial}{\partial x}\left(\frac{\mathrm{M}^2}{D}\right) + gD\frac{\partial \eta}{\partial x} &= 0 \quad , \end{aligned} \tag{8}$$

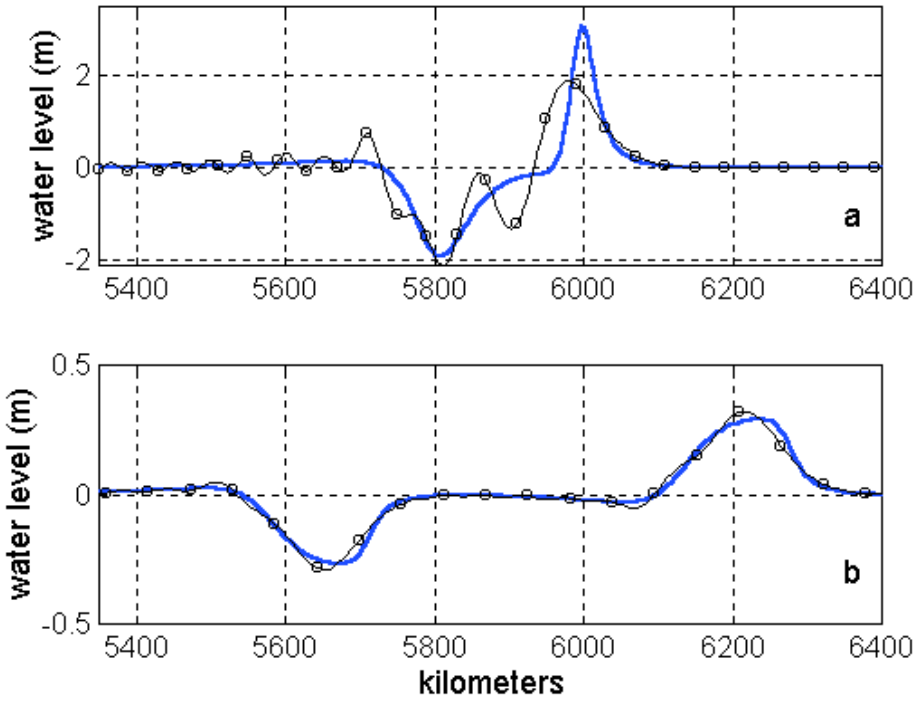

Figure 6: Large tsunami after being propagated a distance of 6000 km from its origin by employing dispersive theory (line with circles) and nondispersive theory (solid line). (a) Along the principal axis and (b) along the diagonal axis.

where $D = \eta + h$.

Equations (8) were solved by an explicit finite-difference scheme described by Goto *et al.* (1997). The grid size was set to 10 m and the time step to 1/20 s. The deep-water tsunami waveforms in Figs. 5a and 6a were propagated to the coast using the bathymetric profile (Fig. 7) taken from the Pacific Central Coast of Mexico, i.e., a near constant ocean depth connected to a deep trench and to a pronounced continental slope, ending in a narrow length continental shelf. The beach slope was assumed to be 5%.

The amplification factors for medium and large tsunamis were 4 and 3, respectively. Thus dispersion is a necessary condition to adequately reproduce the coastal effects, since differences in the height predictions of the leading wave in deep ocean can produce significant differences in coastal run-up. Thus, for the large tsunami (Fig. 6a), overestimations of up to 3 m in run-up can occur with the non-dispersive theory. The oscillatory tail shown in Figs. 5a and 6a, caused by frequency dispersion, can contribute to producing a significant difference between the predictions of dispersive or non-dispersive theories, as the oscillations interacting with the continental slope can produce a resonance pattern with a maximum amplitude occurring several minutes after the arrival of the leading wave. This may be a cause of the resonance pattern observed in Kahului and Hilo, as we will see later (Figs. 11b and 12).

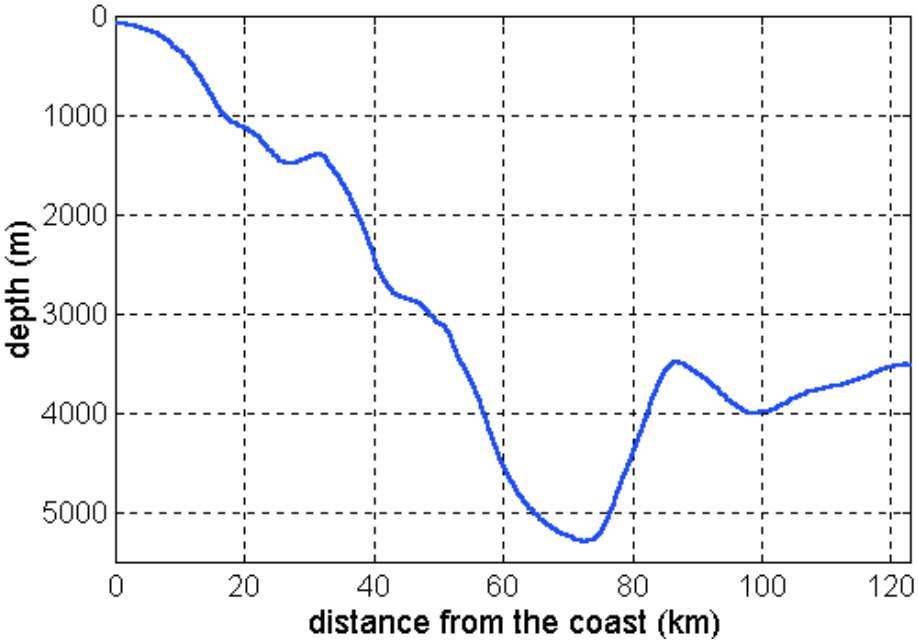

Figure 7: Employed bathymetric profile to propagate the deep-water tsunami waveforms in Figs. 5a and 6a, to the coast.

Finally, when Boussinesq equations are solved by finite difference methods, the solution will contain effects of strong numerical dispersion and dissipation introduced by the finite difference representation of the higher-order derivatives. The overall effect will be to underestimate the height of the leading wave as opposed to the analytical solution. Figure 8 illustrates a particular example, where the solution obtained by finite differences underestimates by ∼30% the height of the leading wave with respect to the height obtained for the analytical solution.

4. A Simplified Model for Transoceanic Tsunami Propagation

The numerical simulation of transoceanic tsunamis requires a major computational effort to provide real-time tsunami warnings. A one-dimensional method to estimate the height of the leading wave is proposed here, not instead of, but in addition to early tsunami warnings.

Two-dimensional axisymmetric long-wave propagation in an ocean of constant depth, without considering Earth rotation, is represented by the one-dimensional zero-order Bessel equation obtained from equations (1) in polar coordinates (r, θ). The classical solution is (Lamb, 1932):

$$\eta(r,t) = \sum_n B_n J_0(k_n r) \cos(\omega t) \ , \tag{9}$$

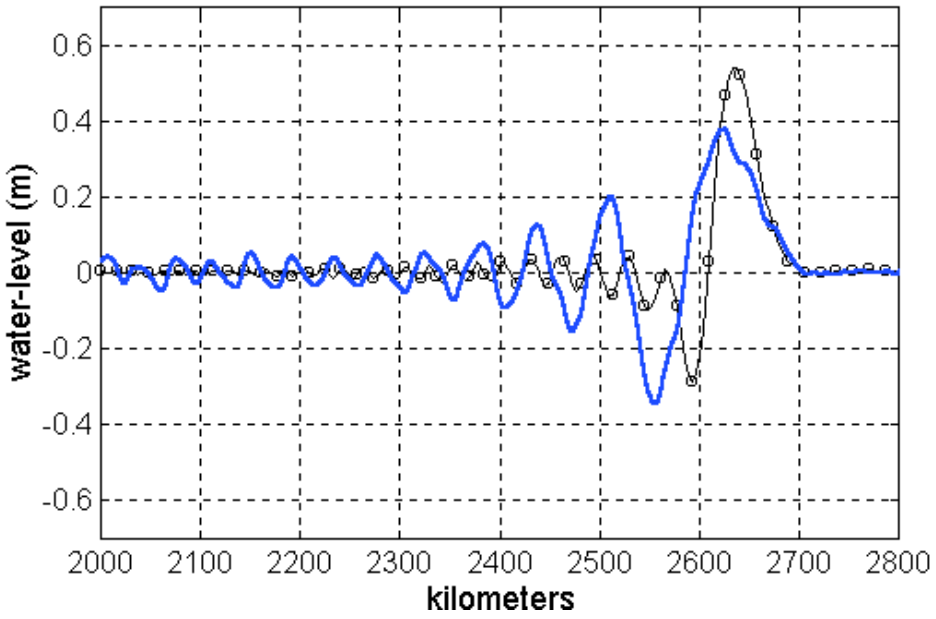

Figure 8: One-dimensional propagation of the medium size tsunami after being propagated a distance of 2700 km from its origin: By means of the analytical solution of Boussinesq equations by Fourier series (line with circles) and by the numerical solution of Boussinesq equations by the finite difference method (solid line).

where J_0 is the Bessel function of zero order and r is the radial distance from the origin of the disturbance. The damping function, H, due to two-dimensional wave spreading, is given by the modulus of the Hankel function:

$$H(k,r) = \sqrt{\frac{2}{\pi k r}} \; . \tag{10}$$

Since the directivity of the tsunami depends on the rupture length, L, and on θ, the damping function can be modified by introducing a suitable directivity function, $\beta(L,\theta)$, that measures the departure from axisymmetric wave spreading:

$$\tilde{H}(k,r) = \sqrt{\frac{2}{\pi k r \beta}} \; . \tag{11}$$

Figure 9 illustrates the directivity function obtained numerically from comparison of the two-dimensional tsunami propagation obtained by means of (6) and (7) with one-dimensional propagation obtained by means of (8). The nonlinear term in (8) was dropped, and the Imamura number was set to 0.6. In the experiments, L was varied between 100 km and 1000 km at steps of 50 km, while W was set to L/4. The principal axis was oriented at $\theta = 90°$. The directivity function was assumed at $r = 6000$ km for values of θ from 0° to 90° at steps of 10°. In all experiments the wavelength of the leading wave is $\sim 2W$; thus the energy spectrum will be concentrated

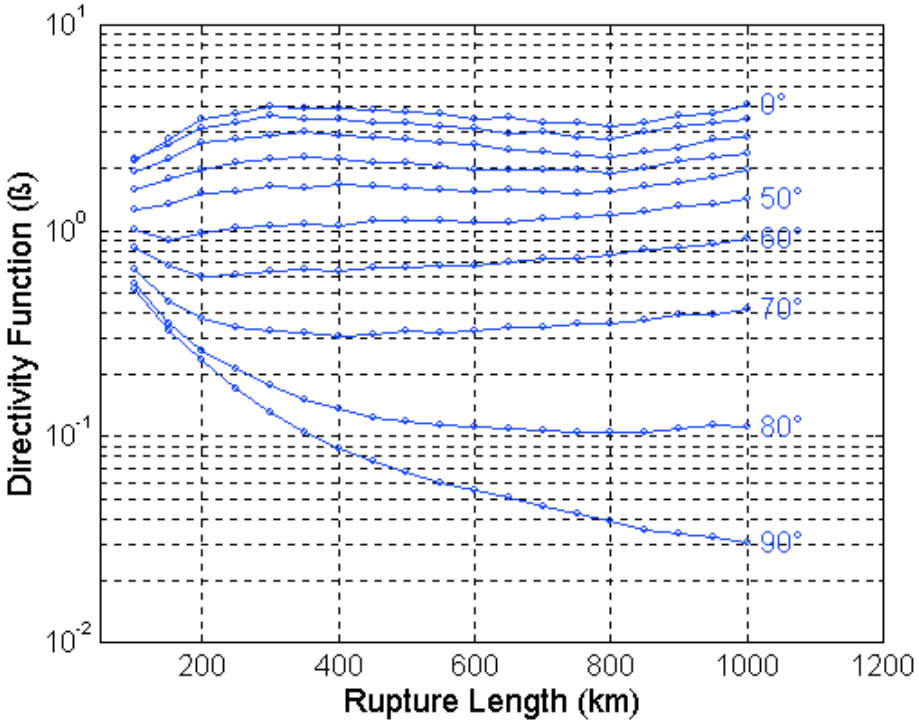

Figure 9: Directivity function, $\beta(L,\theta)$; $\theta = 90°$ is the direction of the principal axis. Numbers in degrees indicate the angle θ.

around $k_0 = \pi/W$. Therefore, the directivity function can be taken as an estimate for the most significant wavenumber, $k = k_0$. This approximation has the advantage of having a single spectral value of $\tilde{H}$ for correcting the amplitude in results obtained with the one-dimensional model. Summarizing, the damping function becomes a damping factor that can be estimated as a function of the directivity, β, the rupture length, L, and the distance, r, from the source along the path S:

$$\tilde{H}(L,r,\beta) = \sqrt{\frac{L}{2\pi^2 r\beta(L,\theta)}} \tag{12}$$

Figure 10a shows a synthetic tsunami, $\eta(r_0,t)$, computed at the location of the BPR by one-dimensional propagation of the Shikotan tsunami along the path S, shown in Fig. 1. Figure 10b compares the BPR data and the synthetic tsunami corrected by the damping factor, i.e., $\tilde{\eta} = \tilde{H}\eta(r_0,t)$, where $r_0 = 6370$ km, and the directivity function as taken from Fig. 9 is $\beta(120\text{ km}, 30°)$. There is an excellent agreement between the BPR data and the corrected synthetic tsunami, even when the angle in the directivity function varies from 20° to 40°.

In order to assess the efficiency of the directivity function, the one-dimensional simulation of the 4 October 1994 Shikotan tsunami was propagated along the paths to Wake Island and to Kahului Bay (Hawaii) up to

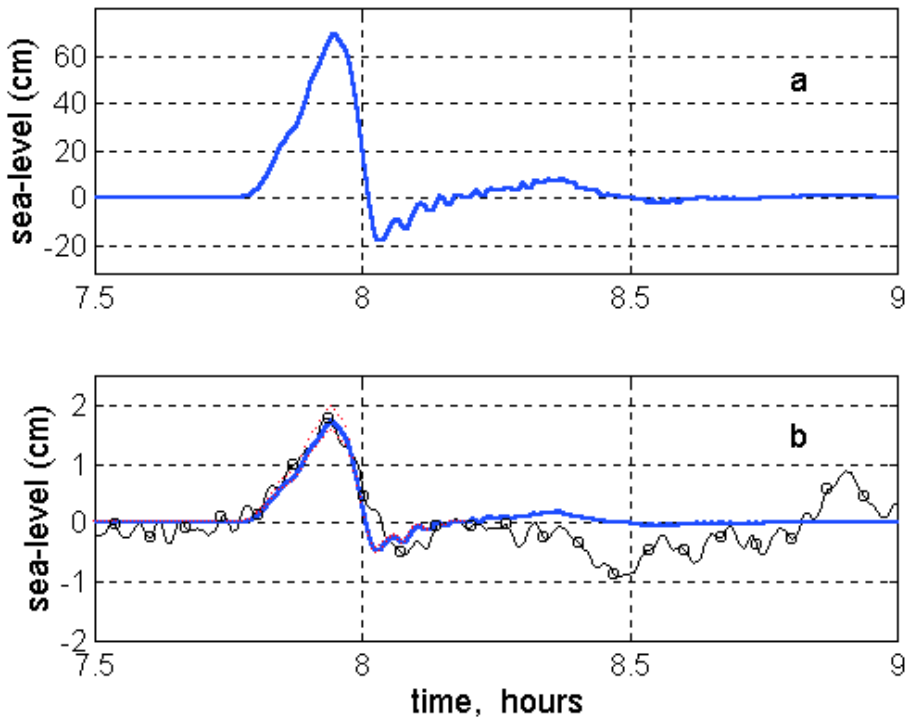

Figure 10: (a) The synthetic 4 October 1994 Shikotan tsunami at the BPR location obtained by the one-dimensional model without considering the directivity function. (b) Comparison of the observed 4 October 1994 Shikotan tsunami (BPR data; line with circles) with the synthetic one-dimensional tsunami (solid line) corrected by the directivity function $\beta(120\text{ km},\ 30°)$. Dotted lines correspond to the synthetic tsunami corrected by using $\beta(120\text{ km},\ 20°)$ and $\beta(120\text{ km},\ 40°)$. The origin of the time axis is defined as the origin time of the earthquake.

a depth of 10 m. The leading wave of the synthetic tsunami is only 2 cm (∼20%) larger than that observed at Wake Island (Fig. 11a). The directivity function was taken as $\beta(120\text{ km}, 90°) = 0.44$, and $r_0 = 3200$ km. Both the amplitude of the leading wave and the following oscillations reproduce approximately the amplitude and periods of the observed tsunami. Since the shape of the harbor cannot be represented in the one-dimensional model, the results suggest that the resonance period (∼14 min) observed at Wake Island is primarily due to the steep grade of the island slope into the deep-ocean. The travel time (∼7 min) for a barotropic wave from the coast to the edge of the island slope was computed from the bathymetric profile and is consistent with the resonance period.

Kahului Bay was chosen as an extreme test for the one-dimensional model. This is a v-shaped Bay that will increase the amplitude of any incoming plane wave front; it is located in a caustic region of ray convergence for this particular tsunami (see Fig. 1). Figure 11b shows a comparison between the observed and synthetic tsunami at Kahului. The directivity function was taken as $\beta(120\text{ km}, 45°) = 1.13$, and $r_0 = 5700$ km. The observed amplitude

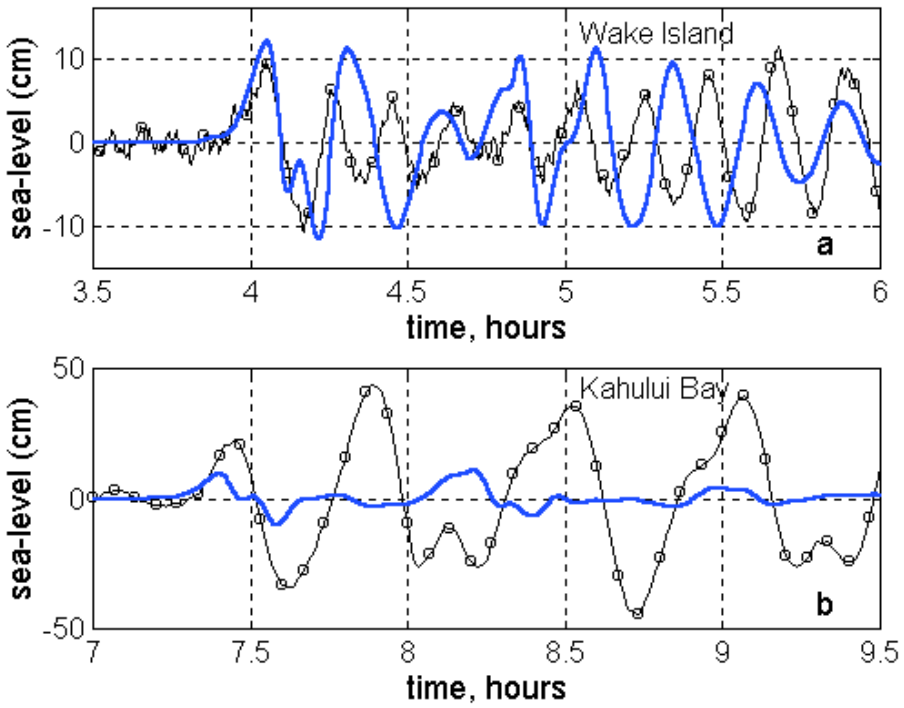

Figure 11: (a) Comparison of the observed 4 October 1994 Shikotan tsunami in Wake Island (line with circles) with the synthetic one-dimensional tsunami (solid line) corrected by using the directivity function $\beta(120\text{ km}, 90°)$. (b) Comparison of the observed 4 October 1994 Shikotan tsunami in Kahului Bay, Hawaii (line with circles) with the synthetic one-dimensional tsunami (solid line) corrected by using $\beta(120\text{ km}, 45°)$. The origin of the time axis is defined as the origin time of the earthquake.

of the leading wave is 10 cm (∼50%) larger than the synthetic amplitude. Hence the local response of the bay must be determined in advance if this method is going to be used for real-time warning purposes; otherwise it will underestimate the wave heights at the coast.

As an example of the simulated one-dimensional large tsunami, the 1964 Alaska tsunami was propagated to Hilo, Hawaii. In Fig. 12, the one-dimensional method reproduces adequately the leading wave recorded at Hilo. The bathymetric profile from the source to Hawaii was taken along the path that joins Hilo and the center of the rupture (150°W, 59°N). The directivity function was taken as $\beta(800\text{ km}, 40°) = 1.55$, while $r_0 = 4400$ km. As in the case of Wake Island, the later oscillations in the synthetic tsunami at Hilo can be considered as evidence that the resonance period (∼40 min) is due to the island slope. The travel time (∼20 min) from the coast to the edge of the slope is consistent with the resonance period.

The one-dimensional model proposed here can be used as a complementary approach to evaluate the risk of potential tsunami flooding. It takes only 2 minutes of CPU time in a Pentium-I processor to propagate a tsunami

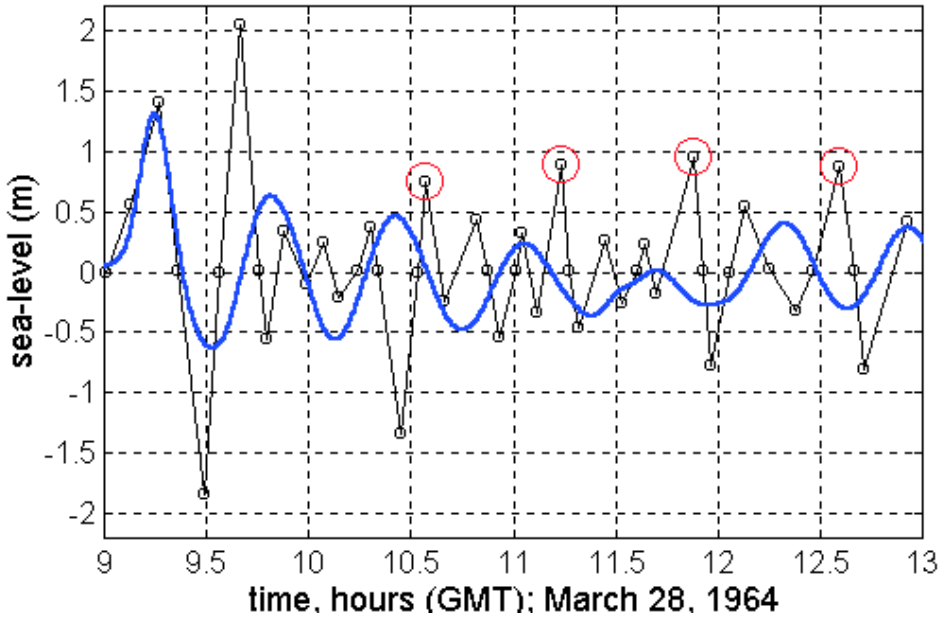

Figure 12: Observed 28 March 1964 Alaskan tsunami in Hilo, Hawaii (line with circles) and the synthetic one-dimensional tsunami (solid line) corrected by using the directivity function β(800 km, 40°). Wide circles on the peaks of the observed tsunami indicate the resonance period (∼40 min).

from Alaska to Hawaii. For any particular region of interest (e.g., Tsunami Reception Region, TRR), the method requires a single two-dimensional numerical tsunami propagation departing from the TRR in order to obtain the travel-time matrix. The tsunami initial condition can be a Gaussian surface. Once the travel-time matrix is obtained, the paths S and the corresponding bathymetric profiles can be obtained for every tsunami-generating region. They can be stored in separate files named for the coordinates of the tsunami-generation region. An algorithm based on the rupture parameters and on the epicenter location can compute the one-dimensional tsunami initial condition and propagate it along the selected pre-computed path. The angle, θ, can be chosen as 90° or 45° in order to have an early estimation of the expected maximum and medium wave height in deep ocean near the TRR. The one-dimensional tsunami signal in deep-ocean can be used as an input for two-dimensional near-shore tsunami propagation and run-up. The directivity function may be improved and tested for every particular TRR. The validity of the directivity function is conditioned to the absence of caustic regions where tsunami convergence is expected.

5. Discussion and Conclusions

The frequency dispersion mechanism of tsunami propagation has been found for the deep-ocean signature of the Shikotan tsunami as well as for the evo-

lution of large and medium-size tsunamis, by comparing the linear dispersive model with the linear non-dispersive model.

1. Frequency dispersion as prescribed by the Boussinesq equations is a necessary and sufficient condition for the propagation of large and medium-size tsunamis.

2. The analytical solution of the Boussinesq equations, or the numerical solution of shallow water equations (setting the Imamura number close to unity) should be used as the most adequate governing equations for transoceanic tsunami propagation.

3. The use of a simplified one-dimensional method with a proposed directivity function in early tsunami warning systems may significantly improve the wave-height predictions in real time, when the local response and the bathymetry for each location are known in advance.

Acknowledgments. We thank F.I. González for valuable BPR tsunami data and for sea-level records of Wake Island and Kahului, Hawaii. We thank S. Farreras and V. Kostoglodov for their comments and review of the manuscript

6. References

Anderson, J.G., P. Bodin, J.N. Brune, J. Prince, S.K. Singh, R. Quaas, and M. Onate (1986): Strong ground motion from the Michoacán-México earthquake. *Science*, *233*(4768), 1043–1049.

Blackford, M.E. (1999): International responses to Pacific tsunami warnings and watches. In *Proceedings of the International Conference on Tsunamis*, edited by B. Massion, Dépt. d'Analyse, Surveillance et Environment du CEA, Paris, 61 pp.

Eble, M.C., D.M. Mattens, and H.B. Milburn (1989): Instrumentation, field operations and data processing for PMEL deep ocean bottom pressure measurements. *NOAA Technical Memorandum ERL PMEL-89* (NTIS PB90-114018), Pacific Marine Environmental Laboratory, Seattle, WA, 71 pp.

Eble, M.C., and F.I. González (1991): Deep-ocean bottom pressure measurements in the northeast Pacific. *J. Atmos. Oceanic Technol.*, *8*, 221–233.

González, F.I., E.N. Bernard, H.B. Milburn, D. Castel, J. Thomas, and J.M. Hemsley (1987): The Pacific Tsunami Observation Program (PacTOP). *Proc. 1987 Int. Tsunami Symp.*, Vancouver, IUGG, 3–19.

Goto, C., Y. Ogawa, N. Shuto, and F. Imamura (1997): IUGG/IOC TIME Project: Numerical Method of Tsunami Simulation with the Leap-Frog Scheme, Intergovernmental Oceanographic Commission of UNESCO, Manuals and Guides #35, Paris, 4 Parts.

Hammack, J.L., and H. Segur (1978): Modelling criteria for long water waves. *J. Fluid Mech.*, *84*, part 2, 359–373.

Heinrich, P., F. Schindele, and S. Guiborg (1998): Modeling of the February 1996 Peruvian tsunami. *Geophys. Res. Lett.*, *25*(14), 2687–2690.

Houston, J.R. (1978): Interaction of tsunamis with the Hawaiian Island calculated by a finite-element numerical model. *J. Phys. Oceanogr., 8*(1), 93–102.

Houston, J.L., and H.L. Butler (1984): Numerical Simulations of the 1964 Alaskan Tsunami. Nineteenth Coastal Engineering Conference, *ASCE. Proc. of the International Conference*, *1*, 815–830.

Imamura, F., N. Shuto, and C. Goto (1990): Study on numerical simulation of the transoceanic propagation of tsunamis—Part 2, Characteristics of tsunami propagating over the Pacific Ocean. *Zisin (J. Seismol. Soc. Japan)*, *43*, 389–402.

Kanamori, H., and J.J. Ciper (1974): Focal process of the great Chilean earthquake, May 22, 1960. *Phys. Earth Planet. Int., 9,* 128–136.

Kikuchi, M., and H. Kanamori (1995): The Shikotan earthquake of October, 1994: Lithospheric earthquake. *Geophys. Res. Lett.*, *22*(9), 1025–1028.

Kowalik, Z. (1993): Solution of the linear shallow water equations by the fourth-order leapfrog scheme. *J. Geophys. Res.*, *98*(C6), 10,205–10,209.

Lamb, H. (1932): *Hydrodynamics,* 6th edition, 738, Cambridge Univ. Press.

Liu P.L., Y.S. Cho, S.B. Yoon and S.N. Seo (1995): Numerical Simulations of the 1960 Chilean Tsunami Propagation and Inundation at Hilo, Hawaii. In *Tsunami Progress in Prediction, Disaster Prevention and Warning*, edited by Y. Tsuchiya and N. Shuto, Kluwer Academic Publishers, Netherlands.

Mansinha, L., and E. Smylie (1971): The displacement field of inclined faults. *Bull. Seismol. Soc. Am., 61,* 1433–1440.

Ortiz, M. (2000): Wavelets desde el punto de vista de la Demodulación Compleja, Apéndice-Tesis Doctoral, Universidad Autónoma Metropolitana-CBI-IPH, México, D.F.

Ortiz, M., S.K. Singh, J. Pacheco, and V. Kostoglodov (1998): Rupture length of the October 9, 1995 Colima-Jalisco earthquake (M_w 8) estimated from tsunami data. *Geophys. Res. Lett., 25*, 2857–2860.

Pedlosky, J. (1979): *Geophysical Fluid Dynamics*. Springer-Verlag, 624 pp.

Satake, K., J. Bourgeois, Ku. Abe, Ka. Abe, Y. Tsuji, F. Imamura, Y. Iio, H. Katao, E. Noguera, and F. Estrada (1993): Tsunami fields survey of the 1992 Nicaragua earthquake. *Eos Trans. AGU, 74*(13).

Satake, K., and F. Imamura (1995): Tsunamis: Seismological and disaster prevention studies. *J. Phys. Earth*, *43*, 259–277.

Shuto, N., C. Goto, and F. Imamura (1991): Numerical simulation as a means of warning for near field tsunamis. In *2nd UJNR Tsunami Workshop Proceedings*, edited by A.N. Brennan and J.F. Lander, National Geophysical Data Center, Boulder, Colorado, 133–153.

Shuto, N. (1991): Numerical simulation of tsunamis—Its present and near future. *Natural Hazards*, *4*, 171–191.

Smith, W.H.F., and D.T. Sandwell (1997): Global seafloor topography from satellite altimetry and ship depth soundings. *Science, 277*(5334), 1956–1962.

Tuck, E.O. (1979): Models for predicting tsunami propagation. In *Tsunamis, Proceedings of the National Science Foundation Workshop*, edited by L.S. Hwang and Y.K. Lee, Tetra Tech Inc., Pasadena, California, 43–109.

Yeh, H., F. Imamura, C. Synolakis, Y. Tsuji, P. Liu, and S. Shi (1993): The Flores Island tsunamis. *Eos Trans. AGU, 74*(369).

Yoon, S.B., and P.L.F. Liu (1993): Numerical simulation of distant small-scale tsunami. In *Recent Advances in Marine Science and Technology 92*, edited by N. Saxena, PACON International, Honolulu, Hawaii, 67–78.